Advances in Hyperspectral Imaging Technologies for Multi-channel Fiber Sensing

Jay Zakrzewski*, Kevin Didona
Headwall Photonics, Inc., 601 River Street, Fitchburg, MA, USA 01420

ABSTRACT

A spectrograph's design, e.g. the opto-mechanical system beginning at the entrance slit, and ending at the back focal plane position, directly impacts system level performance parameters including the height of the useable aperture, spatial and spectral resolving power, optical throughput efficiency, and dynamic range. The efficiency and integrity of both spatial and spectral input image reproduction within the entire back focal plane area is an often overlooked parameter leading to unnecessary acceptance of sacrificed system level performance. Examples of input images include the slit apertured area of a scene captured by a camera lens, a single optical fiber core located within the entrance aperture area, or a linear array of optical fiber cores stacked along the spatial height of the entrance aperture area. This study evaluates the spectral and spatial imaging performance of several aberration corrected high reciprocal dispersion retro-reflective concentric, as well as aberration corrected Offner imaging spectrographs which produce minimal degradation over a large focal plane. Ray trace images and pixilated area maps demonstrating spatial and spectral reproduction accuracy over the entire back focal plane are presented.

Keywords: spectral imaging, hyperspectral imaging, multi-channel, fiber sensing, spectrograph, Raman imaging, SORS

1. INTRODUCTION

Hyperspectral imaging is a high spatial resolution spectral imaging technique originally developed for military airborne and space applications. It is used to capture a wavelength intensity map of a scene with high spatial resolution. The combination of spectral data and spatial detail enables analysis of color, chemical content, uniformity, quality, and a host of other spectrophotometric sensing applications. These systems were designed to perform under ambient lighting conditions, such as available sun light, and therefore required innovative design consideration on sensitivity, efficiency and dynamic range. Some non-commercial applications of hyperspectral imaging include large area spectral mapping of mineral deposits after tsunami's, jungle canopy screening for camouflage detection determined by the disappearance of the near infrared auto-fluorescent chlorophyll band emitted by live foliage, and friend or foe paint signature identification. Lately, applications have advanced into commercial and industrial applications including food and agriculture, anti-counterfeiting, forensics, tissue scanning, cancer detection, biomedical microscopy applications, nano particle research, hazardous and explosive materials detection, and plastic waste sorting.

Hyperspectral imagers are employed as a scanning "push-broom" imager. For each moment in time, or camera frame capture, the scene observed by an objective lens is imaged onto a tall slit aperture. The scene which fills the slit aperture is re-imaged through the spectrometer with the wavelengths dispersed by a grating onto a 2D Focal Plane Array (FPA) camera such as a CCD. One axis of the FPA (pixel-rows) corresponds to the imaged spatial positions along the slit height, preferably in a 1:1 relationship. The second axis (spectral; pixel columns) corresponds to spectral wavelength, which is preferably linearly dispersed and calibrated.

Each 2D image (frame capture), is digitized by the FPA into a 2D data-array corresponding to the field of view imaged through the slit. While scanning a wide scene, multiple 2D image frame captures are taken while spatially stepping across the desired scene width, and these individual frames are stacked like a deck of cards to produce a data file commonly called a hyperspectral data cube. Each pixels value within this hyperspectral data cube represents the wavelength calibrated spectral intensity of that pixels small field of view on the scene. Figure 1 is a graphical representation of a hyperspectral data cube.

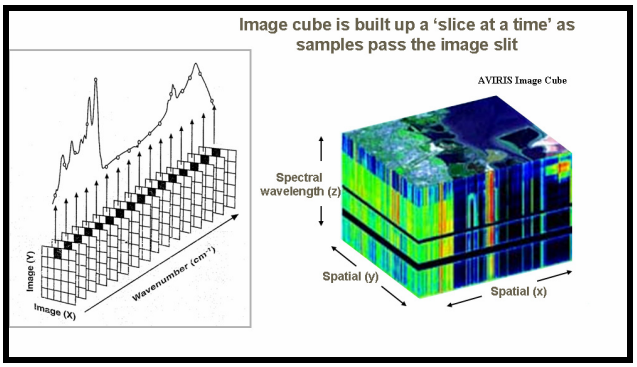

Fig. 1. Hyperspectral data cube (Source: AVIRIS Image Cube)

The resultant three dimensional matrix of data can be analyzed wholly, or interrogated in several ways such as,

1. Vector: spectra at a position X, Y
2. Vector: X-profile at a particular wavelength
3. Vector: Y-profile at a particular wavelength
4. 2D Field: X, Y intensities at a particular wavelength (like a notch-filtered image of any wavelength)
5. Processed into pseudo-color rendered pictures identifying regions where the intensities of a certain wavelength fall within prescribed parameters
6. Processed into pseudo-color rendered pictures identifying regions where a certain spectral signature (spectral-waveform) fall within prescribed parameters

Figure 2 provides an example of the scanning approach in push-broom scanning.

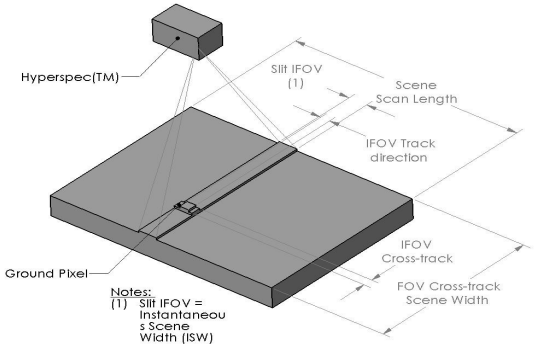

Fig. 2. Push-broom scanning parameters

2. RELAVENCE OF SPECTROGRAPH IMAGING IN MULTI-CHANNEL FIBER SENSING

2.1 Situation

The unique capability of two Headwall Photonics, Inc. hyperspectral imaging spectrometer designs for maintaining precise spatial and spectral integrity of the image located along an entrance slit height ranging from 8 - 18 mm, corresponds to the use of large quantities of discreet optical fibers closely spaced in a linear array along the entrance slit aperture. Spatial and spectral imaging precision minimizes cross talk between each fiber channel, as well as spectral contamination between each spectral channel, resulting in the ability to maximize the number of discrete optical fibers which collect spectral data from a multitude of locations simultaneously.

The quality of both the spectral and spatial input image reproduction at the spectrograph exit focal plane is an often overlooked parameter when selecting an optimized spectrometer design to integrate within a multi-channel fiber optic sensing system. There are various instrument design approaches used for this today, including rack mounting a compact Czerny-Turner f/4 type master spectrometer with several slave optic/detector spectrometer channels operating in a parallel or sequential multiplexed mode, use of a research grade Czerny-Turner imaging (torroidal mirror image compensation) f/4+ spectrometer with a linear array of fiber channels aligned along the entrance slit aperture, as well as use of axial transmissive spectrograph f/1.8+ designs incorporating a series of focusing and collimating lenses along with a planar reflective diffraction grating or a transmissive prism-grating-prism assembly.

Since most optical fiber used today in multi-channel applications is made of fused silica with an N.A. of 0.22, systems faster than f/2.3 do not provide much benefit. Although, one should consider the throughput efficiency comparison between an f/2.3 versus an f/4 design, as the f/2.3 will process 300% more light provided from the optical fiber. This results in significantly increased measurement speed and reduced electronic noise.

2.2 What is meant by "Spectral Image" within a Spectrograph

Relating to fiber optic sensing, an example of a spectrometer input image is an individual fiber core that is positioned at the entrance slit or focal plane. Ideally, one would like to have the shape of this image remain constant after it has been spectrally dispersed and refocused to an array detector aligned to the back focal plane. When viewing a broadband dispersed spectra, it is difficult to visualize a discreet "spectral image" of the fiber core at one wavelength, though in fact there are a continuum of images forming what appears to be a line. One discreet "spectral image" of the fiber core is quantifiable when observing monochromatic spectra. Illumination by an appropriate atomic emission source is an excellent method for this, as the extremely narrow spectral lines represent the reimaged shape of the fiber core for that discreet wavelength. Evaluating the shape and position of these spectral images across the full width of the detector array demonstrates how accurately the fractional rays at different wavelength positions are focused on their intended pixel locations, and how much wavelength corruption may occur when distorted rays fall upon unintended pixel locations.

The ray trace images shown in Figure 3 provide conceptual examples of nominal spectral image distortion. Image A represents a theoretical 50 µm dia. image of uniform intensity at a specific wavelength. At varoius spatial positions over a focal plane, one would like to maintain this shape, or the shape observed in Image B as well as possible. Although, if a spectrograph design perscription is not optimized, aberrations distort the size and shape of the spectral image causing rays intended for that wavelength and spatial position to fall on adjacent locations, thereby corrupting the spectral purity of the measured results. Images C and D provide examples of emerging image distortions, and are minimal in relation to the extent they can degrade in commonly accepted "Research Grade" spectrograph designs. As the data we collected demonstrates, the Raman Explorer does an exceptional job at maintaining high spatial and spectral integrity similar to Image B over the entire focal plane.

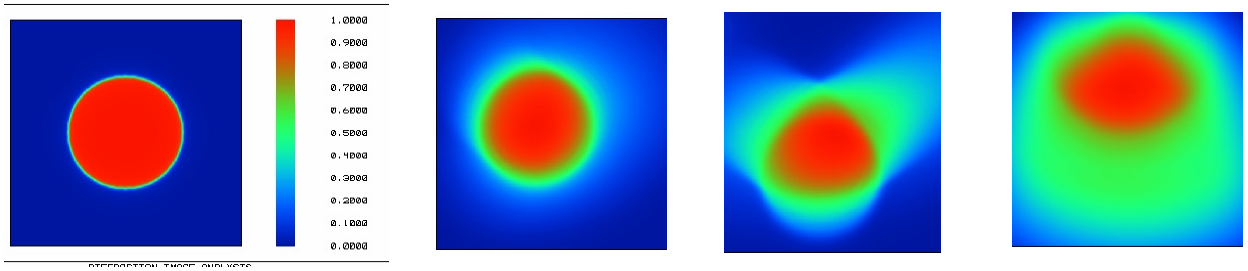

Fig. 3. Conceptual ray trace example of spectral image distortion

2.3 Examples of typical Spectrograph design distortions

2.3.1 Czerny-Turner

Fig. 4

Figure 4 shows an image taken from a 150 mm focal length Czerny-Turner imaging spectrograph which used a torroidal mirror for image correction. Spectral bandwidth is approximately 2000 cm-1 from a 532 nm laser. Two adjacent 50 µm fibers which are separated by the combined 20 µm of cladding and buffer layer were isolated within an array. Note the spatial broadening of the images as wavelength increases left to right. This broadening will cause inaccurate fractional ray blur on adjacent pixels in both the spectral and spatial domains, and contaminate spectral and optical throughput purity.

2.3.2 Single Element Aberration Corrected Concave Grating

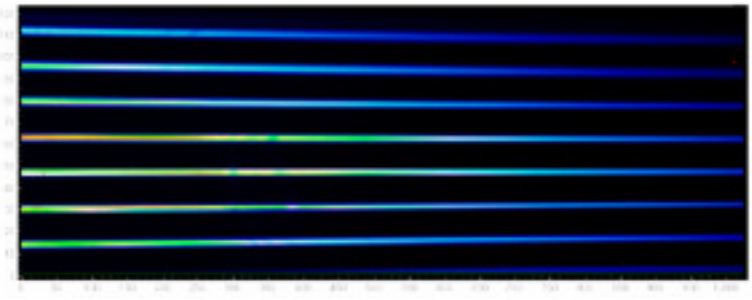

Fig. 5

Figure 5 shows an image taken from a single element aberration corrected concave grating spectrograph. Several live 50 µm core fibers, seperated by five dead fibers each were illuminated with white light. This illustration is a good example of “keystone”, where you can notice the center fiber image disperse parallel to array rows and the closest fiber image neighbors. Although, looking closely, you can see that as the image position moves away from the central sweet spot of the entrance slit, the dispersed images become non-parallel. Ultimately, this limits the usable number of individual fiber channels, and can increase noise during readout. The total hieght of this image was 2.8 mm.

2.3.3 Axial Transmissive

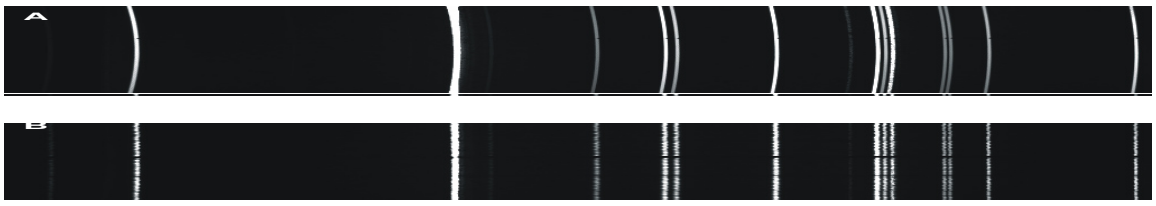

Fig. 6[1]

The top image in Figure 6 shows the resulting curvature of a straight line entrance slit through an axial transmissive spectrograph. The entrance slit was illuminated by an atomic emission source. This is a well understood result of short focal length high numerical aperture spectrograph designs which employ planar gratings. An aberration such as this decreases spectral resolving power, potential signal to noise performance, and creates a challenge with wavelength calibration. Integrators of this type of spectrograph design restrict the input image height to compensate for this

performance issue, resulting in sacrificed signal capture. Others, as demonstrated in the lower image in Figure 6 have compensated for this aberration by laser drilling a custom entrance aperture in the reverse orientation of the parabolic shaped aberrated displacement.

The typical axial transmissive prism-grating-prism (PGP) spectrograph design requires two high quality triplet lenses, one to collimate the light to the PGP element, and the second to focus the dispersed light to the detector. These complex lens designs are necessary to minimize several common aberrations. There is however a cost to performance for this correction. Use of refractive optics over a broad spectral bandwidth results in a loss of resolution due to chromatic aberrations. When a beam of white light hits a lens parallel to the optical axis, the light is refracted differently according to wavelength. The focal point of short wavelength rays is closer to the lens compared to the focal point of longer wavelength light. This is referred to as longitudinal chromatic aberration. The color dispersion can be minimized through the use of compound objectives, one with a high refractive index, and the other with a low refractive index, although optimizing this over a broad wavelength band is difficult. To minimize this effect, the multi-element lenses are constructed using several different glass materials, each having a different refractive index. The dissimilar refractive index of each bonded surface can not be matched by an epoxy, resulting is reflective scattering and losses. Oftentimes, impurities are trapped at the bonding surface layers which can cause additional scattering or non-uniform spectral absorption over the surface area. All air to glass interfaces require an anti-reflective optical coating. Without this coating, losses per surface can reach 4 – 10%. These optical coatings are required to cover a very broad range especially in the case of the SWIR sensor (900 – 2500 nm). Over such a broad range, multiple coating layers are required, the result of which can cause a non-uniform transmission intensity, as well as additional impurities which can cause scatter. Optical anti-reflection coatings only reduce reflections, they do not totally eliminate reflections. Typical performance for broad-band anti-reflective coatings are 0.5 – 1.0 % residual reflectance. The remainder is subject to create ghost and scattering affects. Additionally, each glass material has dissimilar expansion and shifts in refractive index with changes in temperature.

Vignetting is also an important consideration one must fully analyze and understand within any design. In a PGP design, vignetting may occur when lens mounts block the oblique beams causing the edges along the image plane to be incompletely filled with the otherwise available light. This results in the reduction of illumination of the outer parts of the images' field of view. Vignetting may be minimized by increasing the aperture of the lenses, although this also increases size, weight, optical scattering, and cost.

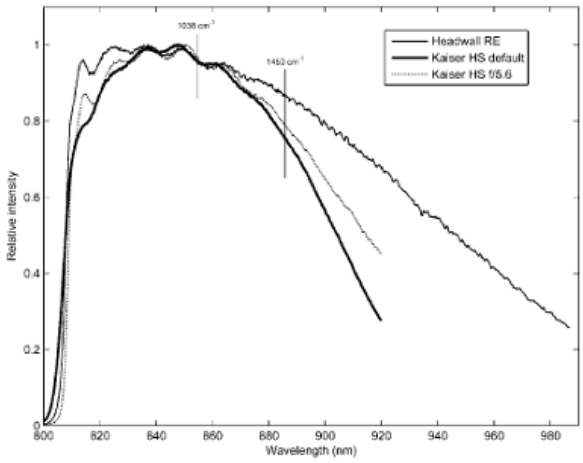

Fig. 7[2]. Vignetting and throughput comparison

An independent throughput comparison of an axial-transmissive spectrograph (Kaiser Holospec™) versus an aberration corrected high reciprocal dispersion retro-reflective concentric spectrograph (Headwall Raman Explorer™) performed at Vanderbilt University shows broadband quartz tungsten halogen lamp spectrum measured with both spectrographs (normalized to maximum intensity). As displayed in Figure 7, throughput of the HS is significantly wavelength dependent compared to the RE. To determine if the throughput degradation was caused by vignetting, the aperture stop

of the internal collimating lens in the axial-transmissive design was adjusted to f/5.6, thereby restricting the light path to the central area of the spectrograph optics. This resulting increase in efficiency at both short and long wavelength extremes is attributed to vignetting, with the residual losses attributed to differences in diffraction efficiency between the transmissive and reflective diffraction gratings used in each instrument design.

3. ADVANCED HYPERSPECTRAL IMAGING SPECTROMETERS

Innovative spectrometer designs originally directed towards hyperspectral imaging techniques have enabled high performance measurement capabilities for a range of multi-channel optical fiber sensors. The following data will demonstrate recent advancements of several highly efficient hyperspectral imaging spectrometer designs that provide precise spectral data simultaneously from high throughput multi-channel fiber optic collection.

3.1 Retro-reflective concentric imaging performance for multi-channel fiber imaging

The Headwall Photonics Raman Explorer™ spectrometer designs emphasize angstrom level spectral resolution over a relatively moderate full spectral bandwidth. The dispersed back focal plane is accurately reimaged over a 26 mm spectral width, and an 8 mm tall spatial height. Therefore, in multi-channel optical fiber sensing applications, the available linear height to stack individual fiber channels is up to a maximum of 8 mm, or approximately one hundred thirty 50 µm core fibers having 10 µm of cladding.

We have performed an evaluation of fine spectral and spatial imaging resolution capabilities and signal throughput characteristics of our Raman Explorer 785 (785 – 975 nm) f/2.4 spectrograph over the area of an Andor Newton camera which included a 2048 x 512 array of 13.5 µm square pixels. This evaluation was originally performed using a 1024 x 256 array of 24 µm square pixels, although the resulting horizontal, vertical, and FWHM imaging was pixel limited. The following is a summary of the 2048 x 512 array results.

To enable imaging of narrow spectral lines, we aligned a test fiber assembly to the entrance aperture. As shown in Figure 8, the test fiber assembly consists of an array of 19 live 50/60/70 µm fibers each separated by 5 dead fibers.

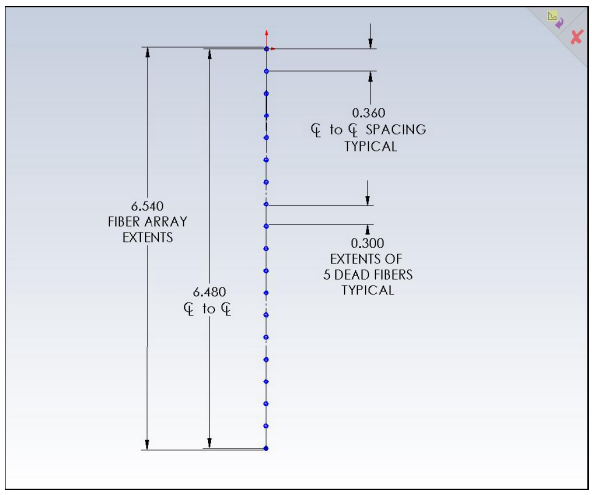

Fig. 8. Test fiber assembly configuration

Raman Explorer™

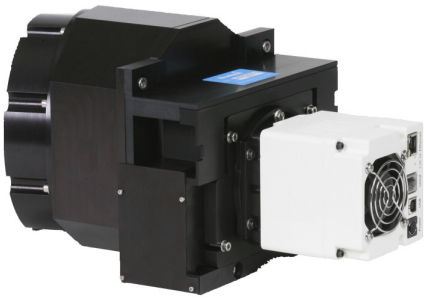

Large area precision focal plane

This fiber assembly allows us to place live 50 µm core fiber images over 6.5 mm of the available 6.9 mm CCD array height at 360 µm center to center distances. Neon and Argon atomic line sources were used to illuminate spectral lines (images) across the full spectral bandwidth of the CCD, then used the following method to capture meaninful spatial and spectral data points:

1. Focused the fiber images and adjusted the light source intensity and camera integration time to just reach, but stay within saturation limits of brightest line. We then set integration time so that readout smear between channels was

minimized, set background subtraction, and captured and stored the image.

2. Same conditions as above, except placing a 10 µm slit over the ferrule face. Take and store image.

In order to provide a baseline illumination for comparison of throughput vs. integration time, an argon pen lamp was inserted into a holder and adjusted so that the 794.82 nm line saturated a pixel within any of the available fiber input/image channels in approximately 0.80 sec. The lamp was then secured in this position.

Using proprietary image test and alignment analysis software developed by Headwall (Figure 9), individual pixel A/D counts were summed in spatial and spectral direction for each fiber image under test. The SUM is divided by the MAX SUM and multiplied by 2^{16} (16 bit) to simulate an integration time which meets the saturation point of the register in a binning application. The pixel A/D count of each fiber image under test was divided by the maximum A/D count within that image and shown in a scale from 1 to 100 and color coded to depict image performance. The spatial and spectral imaging resolution was plotted and the FHWM is measured from the plots and reported.

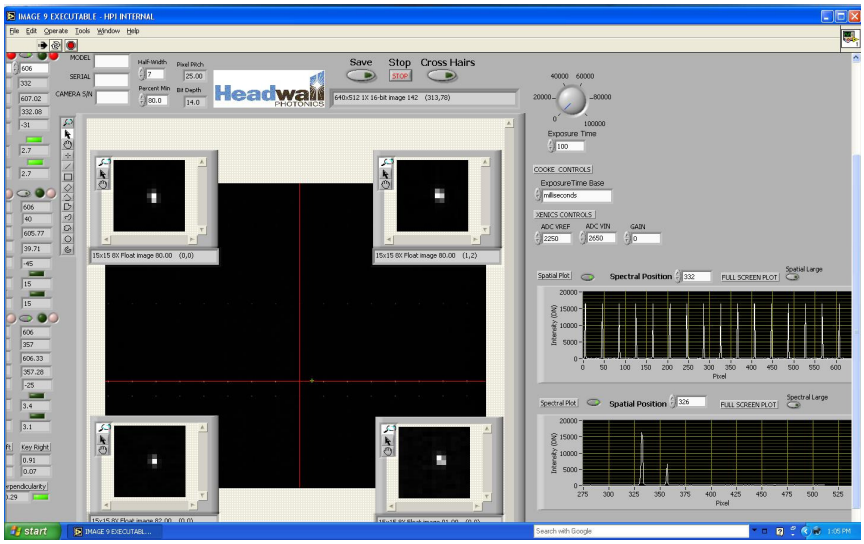

Fig. 9. Headwall Image 9 software

Results of nine 50 µm fiber image positions are shown in Table 1. Three fiber positions along the spatial axis (1, 10, and 19) were selected to demonstrate imaging performance at the top, middle and bottom of the available spatial height, and atomic line wavelength positions 794.82 nm, 842.48 nm, and 965.78 nm were selected along the spectral axis to demonstrate spectral extremes. The color coded pixel maps display the individual pixels' relative intensity and spatial area which covers >/= 50% (FWHM) of the hottest pixel value at near saturation level for that wavelength. Each square in the nine pixelated intensity maps shown represents one pixel, and therefore a perfect FWHM image of a 50 µm core fiber would fill a 4 x 4 pixel area. The horizontal spatial position across the full spectral bandwidth (keystone), and vertical spectral position along the full spatial height of the fiber array (smile), are held within 1 pixel deviation, leading to optimal fiber stacking, wavelength resolution, and calibration accuracy.

Table 1. Nine point pixelated fiber image map

Fiber Optic Test Array, 50 µm fiber core, 60 µm diameter cladding

Wavelength = 794.82 nm
Resolution (FWHM)

Fiber	Spectral		Spatial	
	Pix	nm	Pix	µm
1	3.7	0.33	4.5	60.8
10	3.5	0.32	3.6	48.6
19	4.3	0.39	4.5	60.8

Fiber 1

16	44	64	65	36	8
23	67	94	93	55	17
25	72	100	98	59	22
19	58	89	90	54	19
12	34	52	52	32	13
8	21	28	24	15	7

Fiber 10

9	32	48	34	17	7
25	66	91	78	43	16
33	76	100	99	60	19
23	62	86	78	44	15
8	28	44	34	18	7
2	8	13	12	6	2

Fiber 19

27	38	41	31	17	8
39	62	73	57	34	13
49	85	100	80	49	17
51	86	99	80	51	16
38	63	73	62	37	11
23	33	36	29	16	4

Wavelength = 842.46 nm
Resolution (FWHM)

Fiber	Spectral		Spatial	
	Pix	nm	Pix	µm
1	5.0	0.45	4.8	64.8
10	3.5	0.32	3.6	48.6
19	3.5	0.32	3.6	48.6

Fiber 1

28	49	70	74	63	47
33	58	83	100	94	66
34	61	83	97	94	65
31	53	69	74	70	55
26	41	49	44	31	22
20	30	32	25	14	7

Fiber 10

4	14	24	28	19	8
10	33	61	68	42	17
20	59	95	98	71	33
22	62	94	100	75	41
15	40	67	77	54	21
7	15	25	30	21	8

Fiber 19

5	18	23	17	11	5
15	48	56	43	19	5
33	75	88	77	29	5
39	83	100	91	34	7
25	70	89	76	35	10
9	35	51	45	28	9

Wavelength = 965.78 nm
Resolution (FWHM)

Fiber	Spectral		Spatial	
	Pix	nm	Pix	µm
1	4.6	0.41	5.5	74.3
10	3.5	0.32	4.2	56.7
19	4.0	0.36	3.7	50.0

Fiber 1

29	49	65	60	45	25
36	63	86	88	65	34
37	71	100	100	72	35
33	62	89	95	74	40
26	45	62	65	48	26
21	32	38	36	25	14

Fiber 10

4	14	28	29	17	8
10	36	57	49	30	12
23	72	92	80	40	12
28	76	100	91	47	11
19	60	83	80	37	10
10	29	46	39	21	8

Fiber 19

16	20	25	22	13	6
33	59	70	57	30	13
50	91	100	80	54	20
50	92	96	80	50	14
33	56	62	47	20	5
14	17	17	11	5	2

Pixel Coloring Legend: Green = 50-70% of peak, Yellow = 70-90% of peak, Red = 90-100% of peak

3.2 Hyperspec™ aberration corrected concentric imaging performance for multi-channel fiber imaging

Headwall Photonics latest developments include high efficiency Hyperspec™ NIR (900 – 1700 nm) and SWIR (1000 – 2500 nm) spectrometer designs which emphasize spatial field of view and high efficiency, with good spectral resolution over a relatively wide spectral bandwidth. For application reference, full spectral bandwidths covering 200 – 400 nm, 330 – 825 nm, 380 – 825 nm, 400 – 1000 nm, 600 – 1600 nm, 900 – 1700 nm, and 1000 – 2500 nm are designed.

The patented Hyperspec™ is an all reflective aberration corrected Offner imaging spectrograph design which produce minimal spatial and spectral degradation over a large focal plane. Proprietary developments have now enabled differentiated peak efficiencies in the 90% range (Fig. 10) for high throughput signal processing, as well as athermalization for measurement stability. The Hyperspec is also designed for optimal performance based upon the telecentric entrance pupil formed by an optical fiber.

This evaluation provides performance data of the latest high efficiency Hyperspec™ HE-NIR model. The dispersed back focal plane is accurately reimaged over an 18 mm tall spatial height, and a 4 mm spectral width. Therefore, in multi-channel optical fiber sensing applications, the available linear height to stack individual fiber channels is up to a maximum of 18 mm, or approximately three hundred 50 µm core fibers having 10 µm of cladding.

High Efficiency Hyperspec™ NIR

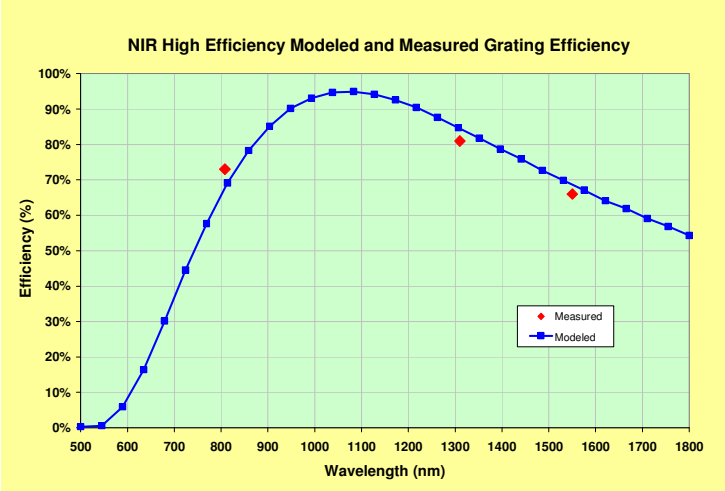

Fig. 10. HE-NIR 900 – 1700 nm modeled and as built diffraction efficiency

Fine spectral and spatial imaging resolution capabilities and signal efficiency characteristics of the Hyperspec™ HE-NIR f/2.4 spectrograph was collected using an integrated Goodrich SU640SDWH-1.7RT InGaAs camera with a 640 x 512 array of 25 µm square pixels.

As displayed in the nine point pixelated table (Table 1), it is critical to maintain tight control of an input image when it is refocused at intended wavelength position on the back focal plane. One measure of this is referred to as ensquared energy. The procedure used for measurement of ensquared energy on the HE-NIR included installing a spectrograph entrance aperture consisting of a linear array of 25 µm pinholes, thereby creating an entrance image matched to the 25 µm pixel pitch on the detector array. The illumination source was an Agilent Technologies 1550 nm tunable laser source.

Table 2. Pixel intensity map

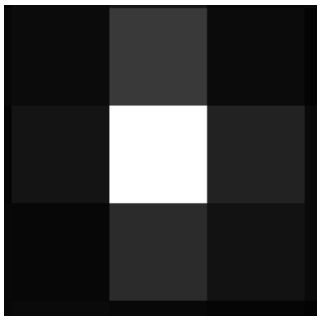

507	2558	484
895	12591	1527
303	1919	831

Fig. 11. 3 x 3, 25 µm pixels

Figure 11 is an enlarged pixel intensity display off the array. Within the central 3 x 3 pixel area, 65% of the light energy launched from the 25 µm pinhole at the entrance aperture is contained within one 25 µm pixel point. Table 2 shows the relative intensity of each pixel. The spatial FWHM results in 1.1 pixels, and the spectral FWHM results in 1.2 pixels.

Spectral image data at 1310 nm and 1550 nm was collected for fourteen pinhole positions over 16 mm of the spatial image height. As Figures 12 and 13 show, smile measured ≤ 0.16 pixels (4 µm) for the total 16 mm spatial height, demonstrating excellent spatial image tracking across the spectral width. This accuracy reduces calibration complexity, and enables increased spectral resolution if binning multiple fibers along the spatial axis. Data collected for one frame, no averaging.

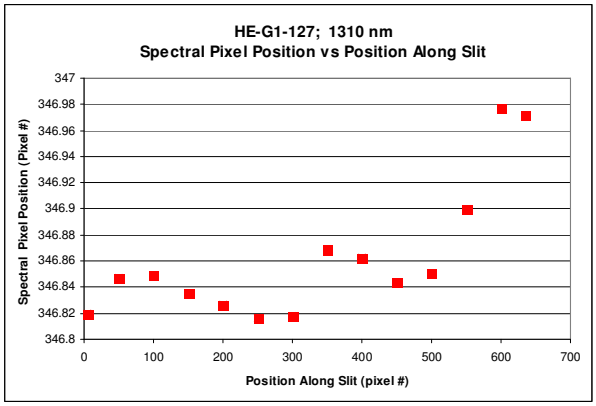

Fig. 12. 1310 nm smile

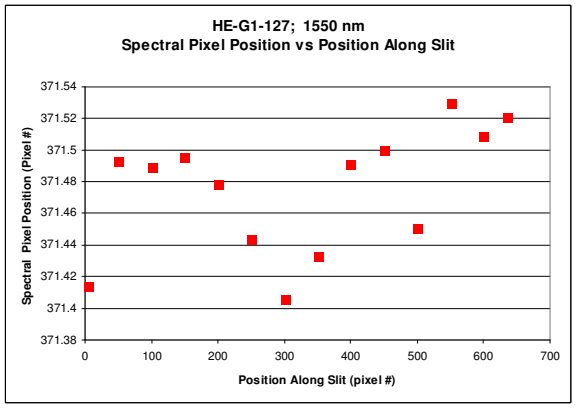

Fig. 13. 1550 nm smile

This same spectral image data was used for investigation of keystone, or the accuracy of which one spatial input image tracks along one spectral pixel row throughout the length of the full spectral band width. Negligible keystone distortion of ≤ 0.04 pixels (1µm) was measured. This level of accuracy minimizes the necessary number of pixels which are binned for each individual fiber channel, and enables a maximum volume of individual fiber channels to be processed.

4. CONCLUSION

Two advanced hyperspectral imaging spectrograph designs were evaluated to demonstrate their potential benefits when applied to multi-channel fiber optic spectral sensing applications. One which emphasizes angstrom level spectral resolution and 8 mm of stackable fiber aperture height, and one which emphasizes up to 18 mm of stackable fiber aperture height and nanometer spectral resolution. Each of these systems demonstrated exceptional accuracy for 1:1 feature imaging, and pixel limited keystone and smile, which optimizes the ability to process a maximum volume of individual channels simultaneously. These systems provide up to 90% efficiency and are matched to the numeric aperture of silica fibers, providing an excellent opportunity for optimizing high throughput measurement results.

REFERENCES

[1] Huang, Z., Zeng, H., "Rapid near-infrared Raman Spectroscopy System for real-time in vivo skin measurements", Optics Letters, Volume 26, No. 22, 1782-1784 (2001)

[2] Lieber, C. A., Kanter, E. M. And Mahadevan-Jansen, A., "Comparison of Raman Spectrograph Throughput Using Two Commercial Systems: Transmissive Versus Reflective", Applied Spectroscopy, Volume 62, Number 5, 575-582 (2008)

For more information contact:

analytikLtd (UK and Ireland Distributor)
2 Cygnus Business Park, Middle Watch, Swavesey, Cambridge, CB24 4AA
T: +44 (0)870 991 4044 E: info@analytik.co.uk **www.analytik.co.uk**